Journal of Electron Spectroscopy and Related Phenomena 201 (2015) 81–87

Contents lists available at ScienceDirect

Journal of Electron Spectroscopy and Related Phenomena

journal homepage: www.elsevier.com/locate/elspec

Tailoring of spin-split metallic surface-state bands on silicon

D.V. Gruznev[a,b], A.V. Zotov[a,b,c], A.A. Saranin[a,b,*]

[a] Institute of Automation and Control Processes, 5 Radio Street, 690041 Vladivostok, Russia
[b] School of Natural Sciences, Far Eastern Federal University, 690950 Vladivostok, Russia
[c] Department of Electronics, Vladivostok State University of Economics and Service, 690600 Vladivostok, Russia

ARTICLE INFO

Article history:
Available online 22 September 2014

PACS:
68.43.Hn
68.37.Ef
68.43.Bc

Keywords:
Atom–solid interactions
Silicon
Rashba effect
Self-assembly
Two-dimensional electron gas
Scanning tunneling microscopy
Angle-resolved photoelectron spectroscopy

ABSTRACT

To exploit Rashba effect in a two-dimensional electron gas on silicon surface for spin devices, it is necessary to have spin-split metallic surface-state bands. However, metals with strong spin-orbit coupling (e.g., Bi, Tl, Sb, Pt) induce reconstructions on silicon with almost exclusively spin-split insulating bands. We suggest to add a second adsorbate to these reconstructions in order to get spin-split metallic bands on silicon. The second adsorbate can affect the surface band structure in two ways. First, it can donate electrons to the available spin-split empty-state insulating or shallow metallic bands converting them to the well-defined metallic bands with enhanced electron filling. Corresponding example systems are Au/Si(1 1 1)$\sqrt{3}\times\sqrt{3}$ modified by In, Tl, Na or Cs and Tl/Si(1 1 1) modified by extra Tl adsorption. Second, by alloying a metal with a strong spin-orbit coupling with the other suitable metal one can obtain a dense two-dimensional alloy layer on silicon which electron band structure contains spin-split metallic bands. For example, this possibility was realized by alloying Bi/Si(1 1 1)$\sqrt{3}\times\sqrt{3}$ reconstruction with Na and Tl/Si(1 1 1)1×1 reconstruction with Pb. The suggested approach allows creation of the metallic surface-state bands with various spin textures on silicon and therefore enhances the possibility to integrate fascinating and promising capabilities of spintronics with current silicon-based technologies.

1. Introduction

The Rashba effect [1,2] which controls formation of a spin-polarized two-dimensional electron gas even in nonmagnetic materials is the key concept of many promising spintronics applications. For utilizing Rashba effect in semiconductor devices to be produced with the silicon-based technologies the requirements as follows have to be satisfied.

- The spin splitting should be large that would allow the device to operate at room temperature.
- The spin-split band should be metallic that would allow significant spin transport.
- The substrate should be a semiconductor that would allow the spin current to be detectable at the background of the non-polarized current through the substrate bulk. Silicon, the most widely used semiconductor material, seems to be the most suitable substrate.
- The layered nanostructure with desirable properties should be easily fabricated using the routine technique, e.g., molecular beam epitaxy.

Among the variety of the known systems with Rashba-type spin splitting of surface-state bands, the overwhelming majority fit only partially the above requirements. For example, the giant spin splitting was first detected on Bi-covered Ag(1 1 1) [3,4] but the substrate here is a metal. The spin-split metallic bands on a semiconductor were found first on Ge surface, namely on the Pb/Ge(1 1 1)$\sqrt{3}\times\sqrt{3}$ [5,6] and Au/Ge(1 1 1)$\sqrt{3}\times\sqrt{3}$ [7–9]. As for the Si substrate, a set of metal-induced reconstructions with Rashba splitting were found, including Bi/Si(1 1 1)$\sqrt{3}\times\sqrt{3}$ [10–12], Tl/Si(1 1 1)1×1 [13–15], Sb/Si(1 1 1)$\sqrt{3}\times\sqrt{3}$ [16] and Pt/Si(1 1 0)"6" $\times$ 5 [17] but in all the cases the spin-split surface-state bands were semiconducting. Thus, in order to create metallic spin-split bands on silicon one has to change somehow the band structure of the metal-induced Si reconstructions. Our suggestion is to employ a second metal adsorbate to reach this goal. As will be shown, a second adsorbate can affect the band structure in two ways. First, adsorbate-induced electron doping of the available insulating empty-state or shallow metallic bands can result in developing well-defined metallic bands with enhanced electron filling. Au/Si(1 1 1)$\sqrt{3}\times\sqrt{3}$ modified by Group-III or alkali metal

* Corresponding author at: Institute of Automation and Control Processes, 5 Radio Street, 690041 Vladivostok, Russia. Tel.: +7 4232310426; fax: +7 4232310452.
E-mail address: saranin@iacp.dvo.ru (A.A. Saranin).

http://dx.doi.org/10.1016/j.elspec.2014.09.006
0368-2048/

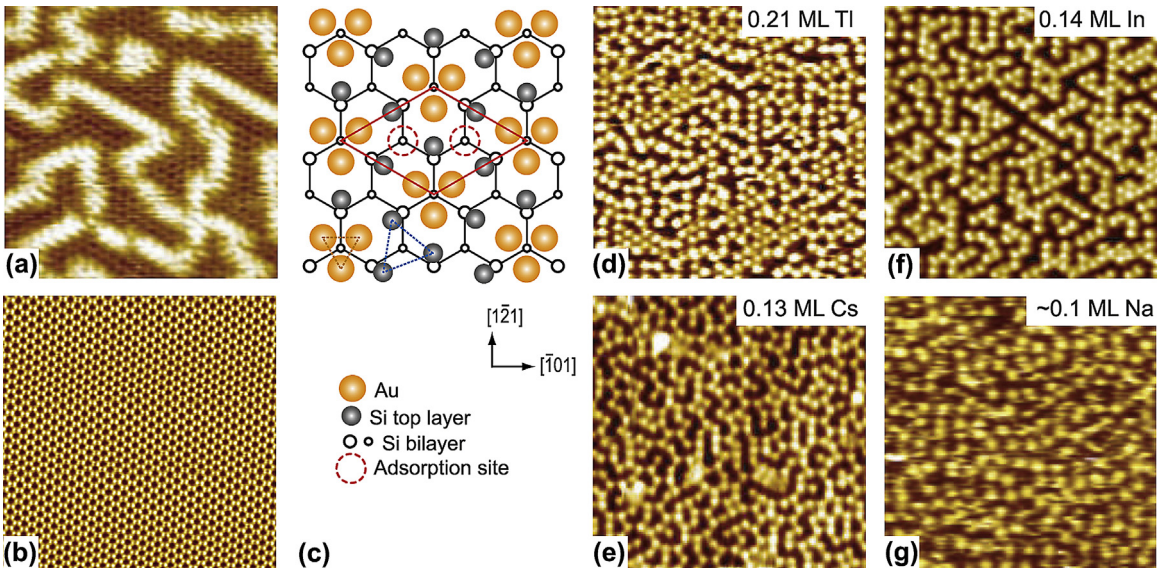

Fig. 1. Structural properties of adsorbate-modified Au/Si(1 1 1)$\sqrt{3} \times \sqrt{3}$ surface. Room-temperature STM images of the (a) pristine and (b) Tl-modified Au/Si(1 1 1)$\sqrt{3} \times \sqrt{3}$ surface. (c) CHCT model of the surfaces where Au atoms are shown by yellow circles, top Si atoms by gray circles, deeper Si atoms by white circles. Adsorption sites of the second adsorbate (In, Tl, Na or Cs) are outlined by dashed red circles. Low-temperature STM images of the Au/Si(1 1 1)$\sqrt{3} \times \sqrt{3}$ surface modified by adsorption of (d) Tl, (e) Cs, (f) In and (g) Na with indicated adsorbate coverage. Scale of all STM images is 170×170 Å^2. (For interpretation of the references to color in this figure legend, the reader is referred to the web version of this article.)

adsorbates and Tl/Si(1 1 1) modified by extra Tl adsorption set the examples. Second, interaction between two metal adsorbates might lead to the formation of a two-dimensional alloy with spin-split metallic bands. Several alloys demonstrating such properties (e.g., Bi–Na and Tl–Pb alloys on Si(1 1 1)) have already been found, the other are awaiting their discovery.

2. Experimental and calculation details

The STM and ARPES experiments were performed in an ultra-high-vacuum Omicron MULTIPROBE system with a base pressure better than $\sim 2.0 \times 10^{-10}$ Torr. Atomically-clean Si(1 1 1)7×7 surfaces were prepared in situ by flashing to 1280 °C after the samples were first outgassed at 600 °C for several hours. Pristine Au/Si(1 1 1)$\sqrt{3} \times \sqrt{3}$ surface was formed by Au deposition onto Si(1 1 1)7×7 surface held at ~600 °C. The adsorbate-modified Au/Si(1 1 1) surfaces were prepared by adsorbing 0.15 ± 0.05 ML (1.0 ML (monolayer) = 7.8×10^{14} cm^{-2}) of a given species, In, Na or Cs, onto the surface held at ~350 °C. Due to significant desorption, deposition of Tl was performed at room temperature (RT) followed by annealing at ~350 °C. Pristine Bi/Si(1 1 1)$\sqrt{3} \times \sqrt{3}$ and Tl/Si(1 1 1)1×1 reconstructions were formed by depositing 1.0 ML of the corresponding species onto Si(1 1 1)7×7 surface held at ~450 °C and ~300 °C, respectively.

STM images were acquired in a constant-current mode. Electrochemically-etched W tips and mechanically cut PtIr tips were used as STM probes after annealing in vacuum. ARPES measurements were conducted using VG Scienta R3000 electron analyzer and high-flux He discharge lamp ($h\nu = 21.2$ eV) with toroidal-grating monochromator as a light source.

Atomic structure of the alloyed (Bi, Na)/Si(1 1 1)$\sqrt{3} \times \sqrt{3}$ and (Tl, Pb)/Si(1 1 1)$\sqrt{3} \times \sqrt{3}$ reconstructions were elucidated using ab initio random structure search (AIRSS) technique [18] after it had been successfully tested for the known Bi/Si(1 1 1)$\sqrt{3} \times \sqrt{3}$ and Tl/Si(1 1 1)1×1 structures.

First-principles calculations were based on DFT as implemented in the Vienna ab initio simulation package VASP, [19,20] using a planewave basis and the projector-augmented wave approach [21] for describing the electron-ion interaction. The generalized gradient approximation (GGA) of Perdew, Burke, and Ernzerhof (PBE) [22] has been used for the exchange correlation potential. The Hamiltonian contains the scalar relativistic corrections, and the spin-orbit interaction was taken into account by the second variation method as has been implemented in VASP by Kresse and Lebacq [23]. To simulate the reconstructions we use a slab consisting of 12 bilayers. Hydrogen atoms were used to passivate the Si dangling bonds at the bottom of the slab. Both bulk Si lattice constant and the atomic positions within the three BLs of the slab were optimized including SOI self-consistently. The silicon atoms of deeper layers were kept fixed at the bulk crystalline positions.

3. Results and discussion

3.1. Adsorbate-induced modification of Au/Si(1 1 1) surface

Structural and electronic properties of the Au/Si(1 1 1)$\sqrt{3} \times \sqrt{3}$ surface have been the object of numerous studies. Its atomic arrangement is commonly accepted to be described by the conjugated honeycomb chained-trimer (CHCT) model [24,25]. In a larger scale, the main characteristic structural feature of the surface is a disordered meandering domain-wall network which separates the commensurate $\sqrt{3} \times \sqrt{3}$ domains [26] (Fig. 1a). Density of domain walls increases with Au coverage [26–28]. As for its electronic properties, the surface is known to be metallic [29], but its metallicity is not strongly expressed: the surface-state spectral features are smeared due to the domain walls and the metallic S_1 surface-state band is shallow, hence its electron filling is rather low, ~0.1 electrons per unit cell [30]. Therefore, though theoretical calculations [25,31] predict that the S_1 band is spin-split, this cannot be resolved in the experimental ARPES spectra from the pristine Au/Si(1 1 1)$\sqrt{3} \times \sqrt{3}$ surface [30].

However, poor structural and electronic properties of the Au/Si(1 1 1)$\sqrt{3} \times \sqrt{3}$ surface substantially improve after adsorbing small amounts of suitable species. This effect was found first for In adsorption [32] and then was spread to other adsorbates, namely Tl, Cs and Na [31,33]. The adsorbate-modified Au/Si(1 1 1) surfaces were prepared by adsorbing 0.15 ± 0.05 ML of a given species, In, Na or Cs, onto the surface held at ~350 °C. Due to significant

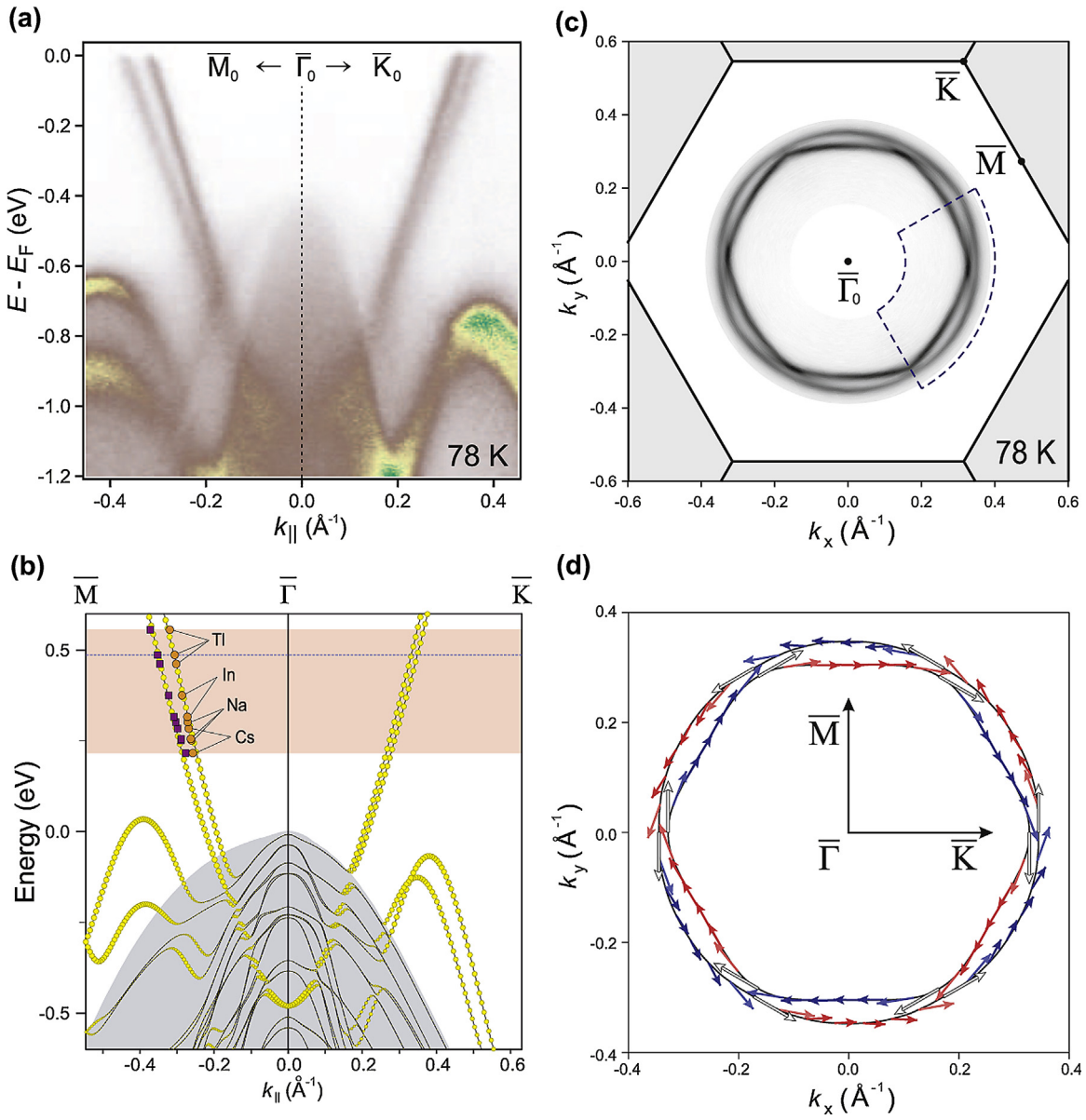

Fig. 2. Electronic properties of adsorbate-modified Au/Si(1 1 1)$\sqrt{3} \times \sqrt{3}$ surface. (a) Experimental ARPES spectrum of Tl-adsorbed Au/Si(1 1 1)$\sqrt{3} \times \sqrt{3}$ and (b) calculated band structure with the experimental dots for various adsorbates superposed on the dispersion curves. Range of the varied Fermi level position is indicated by the pink shaded area. Surface state bands are shown by filled yellow circles, the bulk bands are indicated by shaded region. (c) Symmetrized Fermi surface of Tl-adsorbed Au/Si(1 1 1)$\sqrt{3} \times \sqrt{3}$ surface determined with ARPES. The *k*-space area where the measurements were carried out is outlined by a dashed blue line. (d) Calculated Fermi contours. Small arrows along the Fermi contours and their length indicate the in-plane spin component. The out-of-plane spin component is indicated by the colour of the arrows with red and blue corresponding to the upward and downward directions, respectively. White colour indicates fully in-plane spin alignment. (For interpretation of the references to color in this figure legend, the reader is referred to the web version of this article.)

desorption, deposition of Tl was performed at room temperature followed by brief annealing at ~350 °C. After such a modification, domain walls are completely eliminated and a highly-ordered *h*-$\sqrt{3} \times \sqrt{3}$ surface (*h* means homogeneous) is seen in STM images (Fig. 1b). Consequently, a sharp $\sqrt{3} \times \sqrt{3}$ LEED pattern without any other features develops. It has been recognized that the *h*-$\sqrt{3} \times \sqrt{3}$ surface preserves its original CHCT structure (Fig. 1c) while a second adsorbate, In, Tl, Na or Cs, forms a two-dimensional gas of adatoms [30,32,31,33]. Adatoms are highly mobile at room temperature but they can be frozen in fixed positions upon cooling to ~100 K (except for Cs in which case the freeze-out temperature is ~30 K). The low-temperature STM images (Fig. 1d–g) allow direct determination of the adatom density, which shows that for all adsorbates it falls in the range from ~0.1 to ~0.2 ML. Another common feature of all adsorbates is that the most energetically favorable adsorption site for adatom is the T_4 site over the Si trimer [25,32,33] (Fig. 1c).

ARPES observations demonstrate that upon adding adsorbates all spectral features of the Au/Si(1 1 1)$\sqrt{3} \times \sqrt{3}$ surface are preserved but become noticeably sharp due to removal of domain walls (Fig. 2a). All bands are shifted down towards the higher binding energy. Shifting down is the greatest for the metallic S_1 band that results in increasing its electron filling three to seven times (up to ~0.3–0.7 electrons per unit cell) depending on amount and type of adsorbate. It becomes clearly seen that the metallic S_1 surface state is split. Spin-polarized ARPES measurements confirm that the band is spin-split with opposite spin orientations in the subbands [31]. Fermi surface map displays two contours of which the outer has an almost circular shape while the inner has a shape of a smoothed

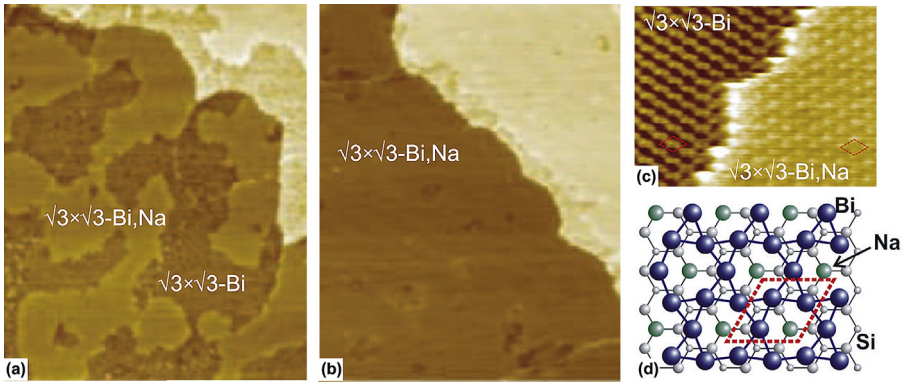

Fig. 3. Formation of the Bi–Na alloy layer on Si(1 1 1). 1600 × 2000 Å^2 STM images illustrating (a) intermediate stage and (b) completion of the Bi–Na layer formation. Note that both STM images show two terraces separated by atomic step. (c) 100 × 75 STM image showing surface area with coexisting domains of pristine Bi/Si(1 1 1)$\sqrt{3} \times \sqrt{3}$ and alloyed (Bi, Na)/Si(1 1 1)$\sqrt{3} \times \sqrt{3}$ phases at a greater magnification. (d) Structural model of the (Bi, Na)/Si(1 1 1)$\sqrt{3} \times \sqrt{3}$ surface where Bi atoms are shown by blue circles, Na atoms by green circles and Si atoms by gray circles. The $\sqrt{3} \times \sqrt{3}$ unit cell is outlined. (For interpretation of the references to color in this figure legend, the reader is referred to the web version of this article.)

hexagon (Fig. 2c and d). As the hexagon corners lies at the $\overline{\Gamma}$–$\overline{K}$ directions, these are the directions of the minimal splitting, while the greatest splitting is at the hexagon sides (i.e., along the $\overline{\Gamma}$–$\overline{M}$ directions).

Fig. 2b summarizes the results for various adsorbate species. All spectra have a qualitatively similar appearance but the splitting value varies. Momentum splitting at the Fermi level $\Delta k_{\|}$ ranges from ~0.018 Å^{-1} obtained for Cs to that of ~0.052 Å^{-1} for Tl. Consequently, energy splitting ΔE_F changes in the range from ~100 meV to ~190 meV. The splitting value is concluded to be essentially controlled by position of the Fermi level, i.e., by the electron filling of the S_1 band. The concept is illustrated in the graph where the experimental dots are superposed on the spin-split dispersion curves of the calculated band structure (Fig. 2b). One can see that by choosing appropriate adsorbate species the Fermi level position can be tuned within the range of ~350 meV (shown by the pink shaded area). Position of Fermi level also varies slightly depending on concentration of a given adsorbate.

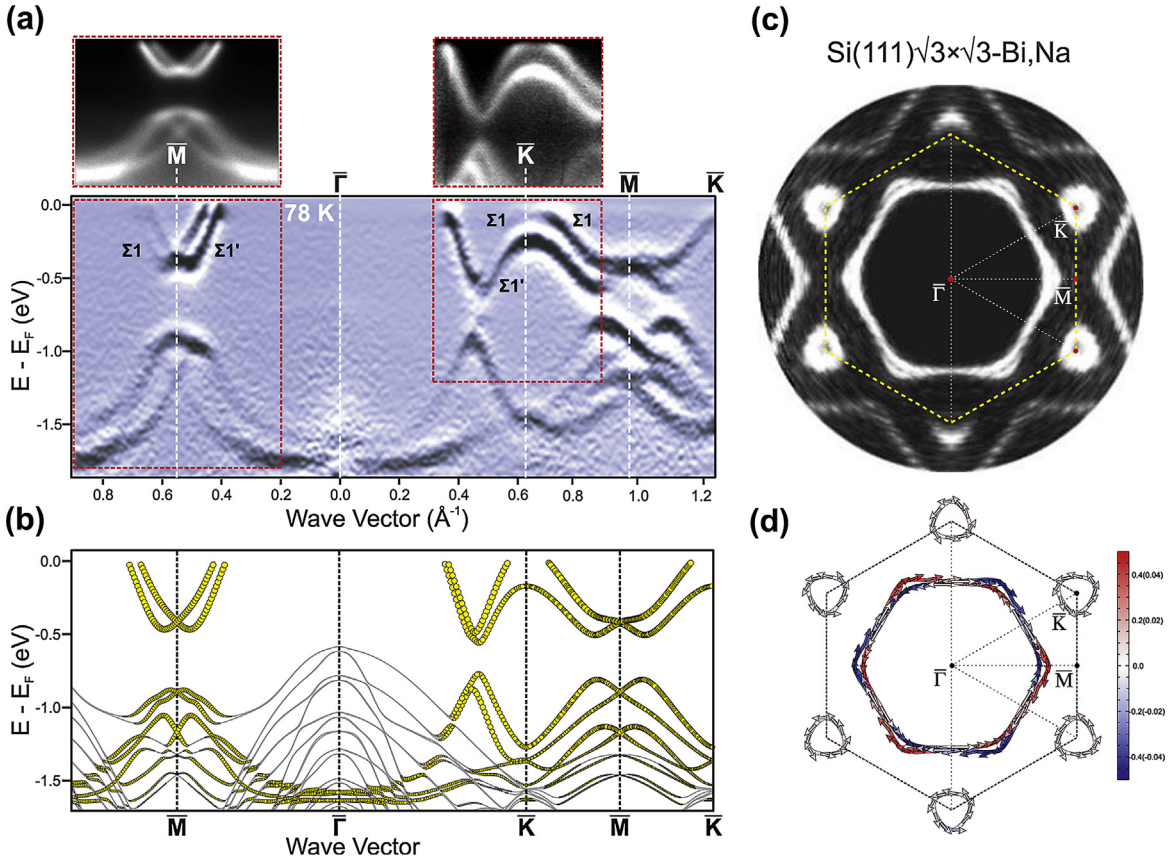

Fig. 4. Electronic properties of (Bi, Na)/Si(1 1 1)$\sqrt{3} \times \sqrt{3}$ surface. (a) Experimental second-derivative ARPES spectrum with outlined regions shown in normal intensity mode and (b) calculated electronic band structure. In the calculated band structure, the size of yellow circles corresponds to the strength of surface character summed over all orbitals at a particular $k_{\|}$ value. (c) Experimental and (d) calculated Fermi contours. The tic values in parentheses in (d) refer to the pocket contours around the $\overline{K}$ points. (For interpretation of the references to color in this figure legend, the reader is referred to the web version of this article.)

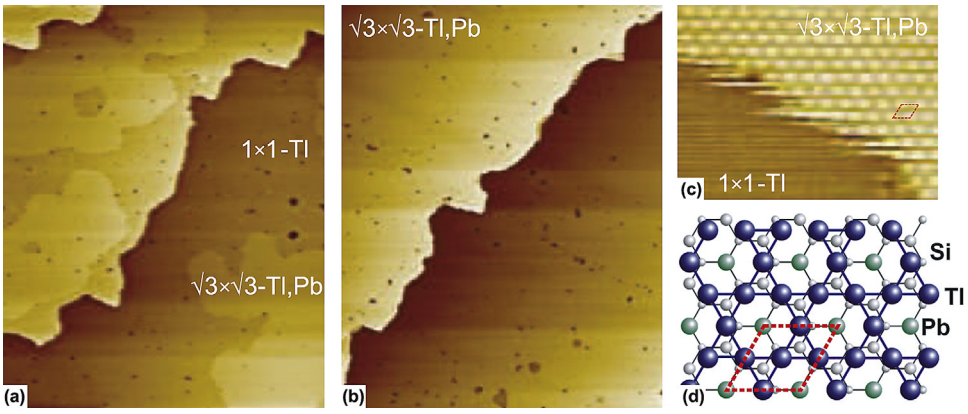

Fig. 5. Formation of the Tl–Pb alloy layer on Si(1 1 1). 1600 × 2000 Å^2 STM images illustrating (a) intermediate stage and (b) completion of the Tl–Pb layer formation. Note that in (a) and (b) there are three and two terraces, respectively. (c) 100 × 75 STM image showing surface area with coexisting domains of pristine Tl/Si(1 1 1)1 × 1 and alloyed (Tl, Pb)/Si(1 1 1)$\sqrt{3} \times \sqrt{3}$ phases at a greater magnification. (d) Structural model of the (Tl, Pb)/Si(1 1 1)$\sqrt{3} \times \sqrt{3}$ surface where Tl atoms are shown by blue circles, Pb atoms by green circles and Si atoms by gray circles. The $\sqrt{3} \times \sqrt{3}$ unit cell is outlined. (For interpretation of the references to color in this figure legend, the reader is referred to the web version of this article.)

Our results show that chemically very different species when being adsorbed onto the Au/Si(1 1 1)$\sqrt{3} \times \sqrt{3}$ surface, affect its structural and electronic properties in a very similar way, namely, eliminate domain walls and donate electrons to the metallic S_1 surface state band. DFT calculations for In-adsorbed surface [32] showed that removal of domain walls is due to a stress-relieving effect produced by In adsorption. We suggest that adsorbates affect the surface lattice stress by donating electrons to the substrate surface layer. As a result, the top layer possesses a non-compensated charge which means adding a Coulomb repulsion term into the interactions between surface atoms, hence changing the surface stress.

3.2. Two-dimensional metal alloys on Si(1 1 1) surface

An alternative way to create a metallic spin-split band on silicon is to form a dense two-dimensional alloy layer containing a metal with strong spin-orbit coupling (e.g., Bi, Tl, Sb, Pt) and another suitable metal. In particular, it is possible to take a certain metal reconstruction on silicon with spin-split semiconducting band and by adding the second adsorbate to form a two-dimensional alloy with spin-split metallic bands. Alloying Bi/Si(1 1 1)$\sqrt{3} \times \sqrt{3}$ reconstruction with Na and Tl/Si(1 1 1)1 × 1 reconstruction with Pb present vivid examples of reaching success with such a technique.

Let us consider first formation of the Bi–Na alloy via deposition of Na onto the β-Bi/Si(1 1 1)$\sqrt{3} \times \sqrt{3}$ surface. The pristine Bi/Si(1 1 1) surface contains 1.0 ML of Bi arranged into the separated trimers centered at the T_4 sites on the bulk-truncated Si(1 1 1) surface [34]. The main features of its electronic structure are spin-split non-metallic bands, $S1$ and $S2$ [10–12]. With Na deposition onto the Bi/Si(1 1 1) surface held at room temperature, the patches of a new phase appear (Fig. 3a and c) and grow in size until covering the whole surface at 0.33 ML of Na (Fig. 3b). The Bi–Na alloy layer preserves the original $\sqrt{3} \times \sqrt{3}$ periodicity of the Bi/Si(1 1 1) phase but it displays a different STM appearance. With knowledge of the alloy composition, 1.0 ML Bi and 0.33 ML Na, we have performed AIRSS to elucidate its atomic structure. The most stable configuration found is shown in Fig. 3d. In this structure, original Bi trimers increase in size by ~8% (Bi—Bi bond length changes from 3.13 to 3.34 Å) and become twisted by ±6.8° [35]. The resultant arrangement of Bi atoms at the surface can be thought then as a honeycomb network of the chained Bi trimers with Na atoms occupying the T_4 sites in the center of each honeycomb unit.

ARPES data and DFT calculations demonstrate that the band structure of the (Bi, Na)/Si(1 1 1) system contains spin-split Σ1 band (Fig. 4a and b) which shows up in the Fermi map (Fig. 4c and d) as two hexagon-shaped contours with corners pointing in the $\overline{\Gamma}$–$\overline{M}$ directions (where the splitting of the band is maximal, momentum splitting $\Delta k_{\parallel} = 0.044$ Å^{-1} and energy splitting $\Delta E_F = 210$ meV). Besides, the Σ1 band forms hole pockets having the shape of smoothed triangles around the $\overline{K}$ points. The out-of-plane spin component for pocket contours is negligible (albeit finite and different for neighboring pockets), the in-plane component dominates and the counterclockwise spin helicity is the same for all six pocket contours [35] (Fig. 4d).

Consider now alloying of the Tl/Si(1 1 1)1 × 1 reconstruction with Pb. The pristine Tl layer contains 1.0 ML of Tl atoms occupying every T_4 site on the bulk-truncated Si(1 1 1) surface [36–38]. The band structure of the Tl/Si(1 1 1)1 × 1 surface includes the spin-split insulating $S1$ band and the shallow metallic $S2$ band around the $\overline{K}$ point [13–15,35,36]. It has been recognized that electron filling of the $S2$ band is associated with extra Tl atoms on the Tl/Si(1 1 1)1 × 1 surface [39] appeared as specific surface defects [40].

Adding 0.33 ML of Pb to the Tl/Si(1 1 1)1 × 1 surface at RT produces a homogeneous Tl–Pb alloy having $\sqrt{3} \times \sqrt{3}$ periodicity (Fig. 6). Its atomic arrangement as determined with AIRSS is shown in Fig. 5b. The Tl atoms form conjugated trimers arranged in a honeycomb network, while Pb atoms occupy T_1 (on-top) sites. Electronic band structure of the Tl–Pb alloy shows a little resemblance with that of the pristine Tl/Si(1 1 1)1 × 1 surface. The most essential newly developed features are the two spin-split metallic surface-state bands, Σ1 and Σ2 (Fig. 6a and b). In the Fermi map of the Σ1 band, the outer contour has almost round shape, while the inner contour is a hexagon with corners pointing in the $\overline{\Gamma}$–$\overline{K}$ directions (Fig. 6c and d). The maximal splitting for the Σ1, $\Delta k_{\parallel} = 0.038$ Å^{-1} and $\Delta E_F = 250$ meV, is along $\overline{\Gamma}$–$\overline{M}$ direction. The second spin-split metallic band Σ2 shows up as hexagonal contours with corners along the $\overline{\Gamma}$–$\overline{M}$ direction, i.e. rotated by 30° compared to the inner contour of the Σ1 band. The maximal splitting for the Σ2 (Σ2′), $\Delta k_{\parallel} = 0.050$ Å^{-1} and $\Delta E_F = 140$ meV, is along $\overline{\Gamma}$–$\overline{K}$ direction.

The shown examples of 2D alloying provide a hint for elucidating the pathways for converting the originally semiconducting surface into the metallic one. Note that both original surfaces, Bi/Si(1 1 1)$\sqrt{3} \times \sqrt{3}$ and Tl/Si(1 1 1)1 × 1, contain 1.0 ML of metal adsorbate. Taking into account that the surface lattice constant of Si(1 1 1) is 3.84 Å, such a density of adsorbate atoms is not sufficient to ensure the overlapping of their electron wave functions. This is typical for metal-induced Si(1 1 1) reconstructions where the atomic layers with metallic properties develop usually when metal coverage exceeds 1.0 ML. For example, In/Si(1 1 1)2 × 2 phase

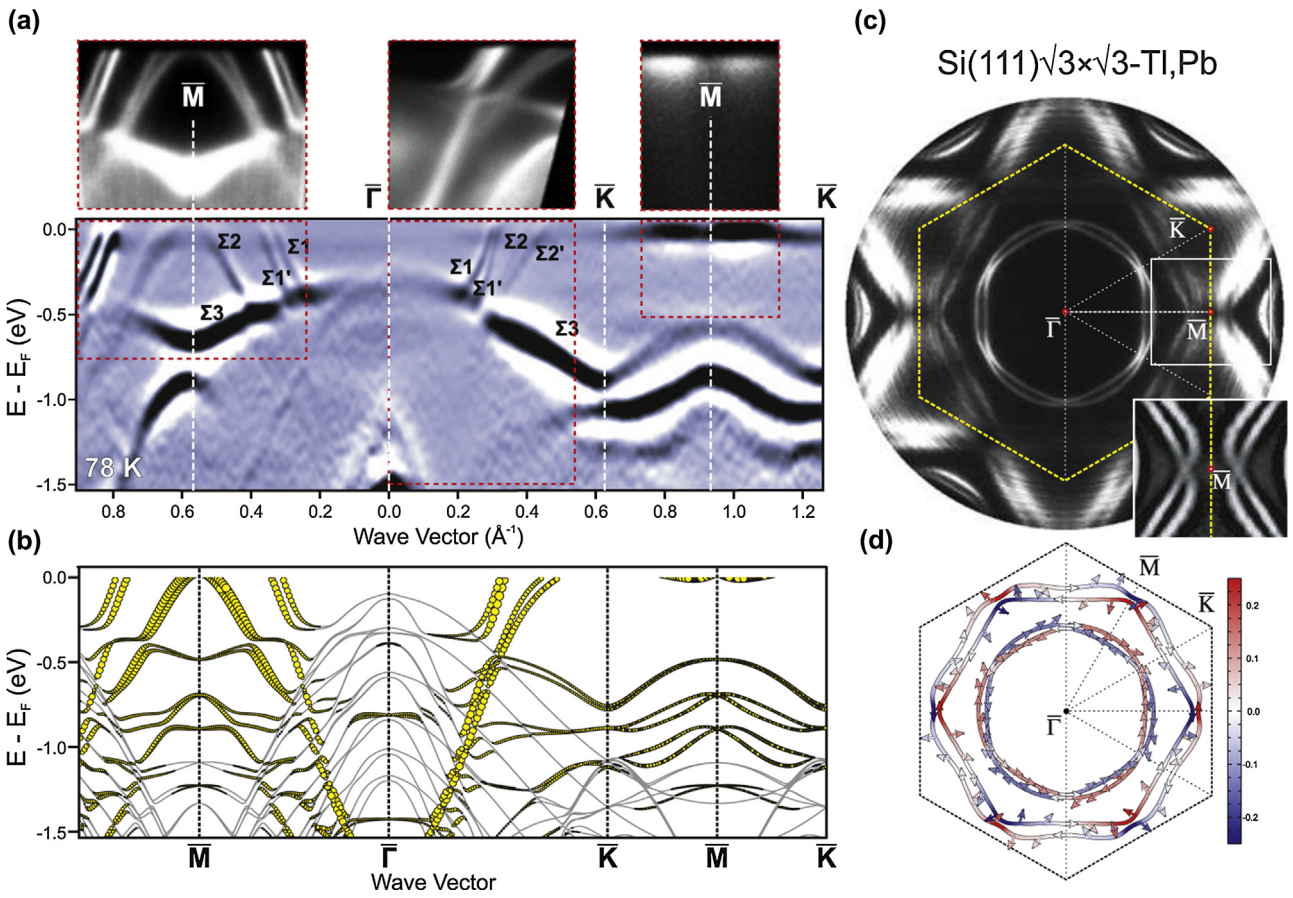

Fig. 6. Electronic properties of (Tl, Pb)/Si(1 1 1)$\sqrt{3} \times \sqrt{3}$ surface. (a) Experimental second-derivitive ARPES spectrum with outlined regions shown in normal intensity mode and (b) calculated electronic band structure. (c) Experimental and (d) calculated Fermi contours. Inset in (c) shows the fine structure within the outlined area around the $\bar{M}$ point with a greater contrast.

with 1.0 ML is semiconducting [41,42] while the In/Si(1 1 1)$\sqrt{7} \times \sqrt{3}$ phases with 1.2 and 2.4 ML In are metallic [43–46]. Another possibility is realized when the metal layer of 1.0 ML is compressed into the interconnected network by Si atoms incorporated within the same reconstructed layer (e.g., as in the case of Ag/Si(1 1 1)$\sqrt{3} \times \sqrt{3}$ containing 1.0 ML Ag and 1.0 ML Si [47,48]). Thus, adding a second metal adsorbate can lead in fortunate cases to the formation of dense ordered alloy layers with delocalized surface states [35]. However, finding an appropriate metal pair is a challenging non-trivial task which requires testing many adsorbate species. Nowadays, the number of the known ordered alloys with spin-split metallic bands on silicon is limited. Besides the (Bi, Na)/Si(1 1 1) and (Tl, Pb)/Si(1 1 1), we can mention also (Bi, Ag)/Si(1 1 1) system [49] where a set of various reconstructions was detected of which the (Bi, Ag)/Si(1 1 1)4 × 4 one contains spin-split metallic band, albeit this band is shallow and its splitting is rather modest. Our preliminary results on (Tl, Bi)/Si(1 1 1) and (Tl, Sn)/Si(1 1 1) have revealed that these systems possess much more advanced spin-related properties. These works are now in progress.

4. Conclusion

In conclusion, we propose an approach for fabricating reconstructions with spin-split metallic surface-state bands on silicon. It resides in taking surface reconstruction which is formed by metal with strong spin-orbit coupling and which band structure contains spin-split insulating or weakly metallic bands and adding a suitable metal adsorbate to it. A set of examples illustrating validity of the approach is presented in the paper. Testing the other promising systems is believed to result in finding new metallic layers with various spin textures which, on the one hand, provide a fascinating playground for exploring spin phenomena in low-dimensional systems and, on the other hand, enhances the possibility to integrate capabilities of spintronics with current semiconductor technology.

Acknowledgements

The authors gratefully acknowledge participation of L.V. Bondarenko, A.V. Matetskiy, A.A. Yakovlev and A.Y. Tupchaya in experimental researches and S.V. Eremeev, J.P. Chou and C.-M. Wei in theoretical calculations and Y.L. Wang and E.V. Chulkov in discussions of the results. The work was supported by Russian Scientific Foundation (Grant 14-02-00479).

References

[1] E.I. Rashba, Sov. Phys. Solid State 2 (1960) 1109.
[2] Yu.A. Bychkov, E.I. Rashba, JETP Lett. 39 (1984) 78.
[3] C.R. Ast, J. Henk, A. Ernst, L. Moreschini, M.C. Falub, D. Pacilé, P. Bruno, K. Kern, M. Grioni, Phys. Rev. Lett. 98 (2007) 186807.
[4] G. Bihlmayer, S. Blügel, E.V. Chulkov, Phys. Rev. B 75 (2007) 195414.
[5] K. Yaji, Y. Ohtsubo, S. Hatta, H. Okuyama, K. Miyamoto, T. Okuda, A. Kimura, H. Namatame, M. Taniguchi, T. Aruga, Nat. Commun. 1 (2010) 17.
[6] K. Yaji, S. Hatta, T. Aruga, H. Okuyama, Phys. Rev. B 86 (2012) 235317.
[7] P. Höpfner, J. Schäfer, A. Fleszar, C. Blumenstein, T. Schramm, M. Heßmann, X. Cui, L. Patthey, W. Hanke, et al., Phys. Rev. B 83 (2011) 235435.
[8] K. Nakatsuji, R. Niikura, Y. Shibata, M. Yamada, T. Iimori, F. Komori, Y. Oda, A. Ishii, Phys. Rev. B 84 (2011) 035436.
[9] P. Höpfner, J. Schäfer, A. Fleszar, J.H. Dil, B. Slomski, F. Meier, C. Loho, C. Blumenstein, L. Patthey, et al., Phys. Rev. Lett. 108 (2012) 186801.

[10] I. Gierz, T. Suzuki, E. Frantzeskakis, S. Pons, S. Ostanin, A. Ernst, J. Henk, M. Grioni, K. Kern, C.R. Ast, Phys. Rev. Lett. 103 (2009) 046803.
[11] K. Sakamoto, H. Kakuta, K. Sugawara, K. Miyamoto, A. Kimura, T. Kuzumaki, N. Ueno, E. Annese, J. Fujii, A. Kodama, T. Shishidou, H. Namatame, et al., Phys. Rev. Lett. 103 (2009) 156801.
[12] E. Frantzeskakis, S. Pons, M. Grioni, Phys. Rev. B 82 (2010) 085440.
[13] K. Sakamoto, T. Oda, A. Kimura, K. Miyamoto, M. Tsujikawa, A. Imai, N. Ueno, H. Namatame, M. Taniguchi, P.E.J. Eriksson, R.I.G. Uhrberg, Phys. Rev. Lett. 102 (2009) 096805.
[14] J. Ibañez-Azpiroz, A. Eiguren, A. Bergara, Phys. Rev. B 84 (2011) 125435.
[15] S.D. Stolwijk, A.B. Schmidt, M. Donath, K. Sakamoto, P. Krüger, Phys. Rev. Lett. 111 (2013) 176402.
[16] X.G. Zhu, Z. Liu, W. Li, J. Wen, X. Chen, J.F. Jia, X.C. Ma, K. He, L.L. Wang, Q.K. Xue, Surf. Sci. 618 (2013) 115.
[17] J. Park, S.W. Jung, M.C. Jung, H. Yamane, N. Kosugi, H.W. Yeom, Phys. Rev. Lett. 110 (2013) 036801.
[18] C.J. Pickard, R.J. Needs, J. Phys.: Condens. Matter 23 (2011) 053201.
[19] G. Kresse, J. Hafner, Phys. Rev. B 47 (1993) 558.
[20] G. Kresse, D. Joubert, Phys. Rev. B 59 (1999) 1758.
[21] P.E. Blöchl, Phys. Rev. B 50 (1994) 17953.
[22] J.P. Perdew, K. Burke, M. Ernzerhof, Phys. Rev. Lett. 77 (1996) 3865.
[23] G. Kresse and O. Lebacq, Technical report, http://cms.mpi.univie.ac.at/vasp/
[24] Y.G. Ding, C.T. Chan, K.M. Ho, Surf. Sci. 275 (1992) L691.
[25] C.H. Hsu, W.H. Lin, V. Ozolins, F.C. Chuang, Phys. Rev. B 85 (2012) 155401.
[26] T. Nagao, S. Hasegawa, K. Tsuchie, S. Ino, C. Voges, G. Klos, H. Pfnür, M. Henzler, Phys. Rev. B 57 (1998) 10100.
[27] J. Nogami, A.A. Baski, C.F. Quate, Phys. Rev. Lett. 65 (1990) 1611.
[28] J. Falta, A. Hille, D. Novikov, G. Materlik, L. Seehofer, G. Falkenberg, R.L. Johnson, Surf. Sci. 330 (1995) L673.
[29] H.M. Zhang, T. Balasubramanian, R.I.G. Uhrberg, Phys. Rev. B 66 (2002) 165402.
[30] J.K. Kim, K.S. Kim, J.L. McChesney, E. Rotenberg, H.N. Hwang, C.C. Hwang, H.W. Yeom, Phys. Rev. B 80 (2009) 075312.
[31] L.V. Bondarenko, D.V. Gruznev, A.A. Yakovlev, A.Y. Tupchaya, D. Usachov, O. Vilkov, A. Fedorov, D.V. Vyalikh, S.V. Eremeev, E.V. Chulkov, A.V. Zotov, A.A. Saranin, Sci. Rep. 3 (2013) 1826.
[32] D.V. Gruznev, I.N. Filippov, D.A. Olyanich, D.N. Chubenko, I.A. Kuyanov, A.A. Saranin, A.V. Zotov, V.G. Lifshits, Phys. Rev. B 73 (2006) 115335.
[33] L.V. Bondarenko, A.V. Matetskiy, A.A. Yakovlev, A.Y. Tupchaya, D.V. Gruznev, M.V. Ryzhkova, D.A. Tsukanov, E.A. Borisenko, E.N. Chukurov, et al., J. Phys.: Condens. Matter 26 (2014) 055009.
[34] R.H. Miwa, T.M. Schmidt, G.P. Srivastawa, J. Phys.: Condens. Matter 15 (2003) 2441.
[35] D.V. Gruznev, L.V. Bondarenko, A.V. Matetskiy, A.A. Yakovlev, A.Y. Tupchaya, S.V. Eremeev, E.V. Chulkov, J.P. Chou, C.M. Wei, M.Y. Lai, Y.L. Wang, et al., Sci. Rep. 4 (2014) 4742.
[36] S.S. Lee, H.J. Song, N.D. Kim, J.W. Chung, K. Kong, D. Ahn, H. Yi, B.D. Yu, H. Tochihara, Phys. Rev. B 66 (2002) 233312.
[37] T. Noda, S. Mizuno, J. Chung, H. Tochihara, Jpn. J. Appl. Phys. 42 (2003) L319.
[38] N.D. Kim, C.G. Hwang, J.W. Chung, T.C. Kim, H.J. Kim, D.Y. Noh, Phys. Rev. B 69 (2004) 195311.
[39] K. Sakamoto, T.H. Kim, T. Kuzumaki, B. Müller, Y. Yamamoto, M. Ohtaka, J.R. Osiecki, K. Miyamoto, Y. Takeici, A. Harasawa, S.D. Stolwijk, et al., Nat. Commun. 4 (2013) 2073.
[40] P. Kocán, P. Sobotík, I. Ošťádal, Phys. Rev. B 84 (2011) 233304.
[41] J.P. Chou, C.M. Wei, Y.L. Wang, D.V. Gruznev, L.V. Bondarenko, A.V. Matetskiy, A.Y. Tupchaya, A.V. Zotov, A.A. Saranin, Phys. Rev. B 89 (2014) 155310.
[42] S.G. Kwon, M.H. Kang, Phys. Rev. B 89 (2014) 165304.
[43] E. Rotenberg, H. Koh, K. Rossnagel, H.W. Yeom, J. Schäfer, B. Krenzer, M.P. Rocha, S.D. Kevan, Phys. Rev. Lett. 91 (2003) 246404.
[44] K. Uchida, A. Oshiyama, Phys. Rev. B 87 (2013) 165433.
[45] J.W. Park, M.H. Kang, Phys. Rev. Lett. 109 (2012) 166102.
[46] S. Yamazaki, Y. Hosomura, I. Matsuda, R. Hobara, T. Eguchi, Y. Hasegawa, S. Hasegawa, Phys. Rev. Lett. 106 (2011) 116802.
[47] T. Takahashi, S. Nakatani, N. Okamoto, T. Ishikawa, Surf. Sci. 242 (1991) 54.
[48] M. Katayama, R.S. Williams, M. Kato, E. Nomura, M. Aono, Phys. Rev. Lett. 66 (1991) 2762.
[49] N.V. Denisov, E.N. Chukurov, Yu.V. Luniakov, O.A. Utas, S.G. Azatyan, A.A. Yakovlev, A.V. Zotov, A.A. Saranin, Surf. Sci. 623 (2014) 17.